Physica A 661 (2025) 130415

Contents lists available at ScienceDirect

Physica A

journal homepage: www.elsevier.com/locate/physa

A multi-scale information fusion approach for brain network construction in epileptic EEG analysis

Zhiwen Ren [a], Dingding Han [a,b,*]

[a] School of Information Science and Technology, Fudan University, Shanghai, 200433, China
[b] Shanghai Artificial Intelligence Laboratory, 701 Yunjin Road, Shanghai, 200232, China

ARTICLE INFO

Keywords:
EEG analysis
Multi-scale information fusion
Brain network dynamics
Network construction
Particle Swarm Optimization
Deep learning

ABSTRACT

Epilepsy is characterized by complex, multi-scale disruptions in brain connectivity, yet most EEG-based network analyses focus on specific frequency bands or time scales, overlooking crucial cross-scale interactions. In this study, we propose a novel multi-scale information fusion (MSIF) framework that integrates connectivity across multiple frequency bands, temporal windows, and construction methods into a single, fused brain network. By employing Particle Swarm Optimization (PSO), our approach adaptively weights each component to maximize seizure–non-seizure discriminability while preserving stability in non-seizure phases. We validated the MSIF framework using two publicly available EEG datasets (CHB-MIT and Siena) and compared its performance against conventional methods. Our results demonstrate that the MSIF framework outperforms single-scale methods, achieving higher Comprehensive Sensitivity Scores (CSS) and more pronounced separation of seizure vs. non-seizure states. Compared to single-scale methods, the multi-scale fusion significantly enhances sensitivity to seizure-induced network reconfigurations, as evidenced by marked alterations in network metrics (e.g., global efficiency, clustering coefficient) during the seizure phase and a clear return toward baseline in post-seizure segments. These findings underscore the potential of multi-scale fusion to provide richer insights into epileptic network behavior and support more accurate seizure detection and monitoring. The proposed framework paves the way for network-based biomarkers in clinical settings, offering a scalable approach adaptable to diverse electrode configurations and patient populations.

Epilepsy is a prevalent neurological disorder characterized by recurrent, unprovoked seizures, affecting approximately 1% of the global population [1,2]. These seizures are commonly associated with abnormal synchronization within brain networks, prompting extensive research into the neural mechanisms underlying these connectivity patterns [3,4]. Electroencephalography (EEG) is widely used in epilepsy research due to its high temporal resolution, allowing for real-time monitoring of brain activity and providing valuable insights into neural interactions across seizure events [5–7]. Analyzing dynamic changes in brain networks during both seizure and interictal (non-seizure) states offers the potential to reveal fundamental aspects of epileptic pathophysiology and improve diagnostic accuracy [8,9].

In the analysis of EEG data, constructing functional brain networks involves estimating connectivity between electrodes or brain regions to capture the dynamic relationships that characterize different brain states [10,11]. Various metrics, such as coherence [12], phase locking value (PLV) [13], and weighted phase lag index (wPLI) [14], are frequently employed to assess connectivity patterns in epilepsy. Additionally, methods like Granger causality (GC) [15] and Dynamic Causal Modeling (DCM) [16] have been applied to infer directional dependencies and causal relationships between brain regions. However, these methods generally focus on

* Corresponding author.
E-mail addresses: renzw23@m.fudan.edu.cn (Z. Ren), ddhan@fudan.edu.cn (D. Han).

https://doi.org/10.1016/j.physa.2025.130415
Received 1 December 2024; Received in revised form 20 January 2025
Available online 6 February 2025

specific frequency bands or temporal scales, potentially missing the complex interactions occurring across multiple scales of neural activity [17–19]. Such single-scale approaches often struggle to capture the full spectrum of brain dynamics, especially in epileptic networks where intricate, multi-scale synchronizations are present [20,21]. Furthermore, thresholding techniques used in traditional methods to eliminate weak connections can introduce variability in network metrics, complicating interpretation and reducing reliability across studies [22,23].

Recently, there has been growing interest in leveraging functional brain network approaches with machine learning to more comprehensively understand and detect abnormal brain activity. For instance, supervised network-based fuzzy learning frameworks have been applied to EEG signals to identify Alzheimer's disease [24], demonstrating the potential of integrating fuzzy modeling with topological features of the network for improved diagnostic accuracy. Meanwhile, the neuromodulatory effects of acupuncture stimulation have been investigated from the perspectives of spectral power and functional connectivity [25]. By constructing functional brain networks and employing advanced machine learning classifiers, different acupuncture manipulations can be discriminated using EEG data [26], thus showing the versatility of network-based methods in detecting and modulating abnormal brain states. Moreover, EEG-based BCIs have advanced with machine learning, improving brain state detection and classification. Techniques have shown potential in adapting EEG patterns for mental state classification [27], achieving high accuracy in emotion recognition [28], and identifying biomarkers for epilepsy and migraine using advanced architectures like BiLSTM and NeuCube [29]. These studies highlight the broader utility of functional brain network analysis combined with robust machine learning strategies, not only in epilepsy but also in other disorders with characteristic brain-network alterations.

Given the intrinsic complexity of epileptic networks, multi-scale EEG network analysis is becoming increasingly important, particularly in the context of epilepsy where neural interactions are inherently multifaceted. Existing multi-scale studies have almost entirely focused on feature fusion in neural networks within the field of deep learning [30,31], while research on information fusion in network construction is significantly limited. Moreover, a consensus has yet to be reached on how best to integrate multi-scale information that spans different frequency bands, temporal windows, and network estimation methods, underscoring the need for more holistic solutions to capture the richness of brain dynamics in epileptic seizures and other brain disorders [32]. Studies on the analysis of EEG frequency bands [33], the selection of temporal windows [18,34], and comparisons of different functional network construction methods [35] are already limited, and investigations into multi-scale information fusion across multiple frequency bands, temporal scales, and functional network construction methods are even more scarce. Achieving effective integration across these scales and methods remains a significant challenge.

In addition, various network metrics such as centrality [36], small-world index [37], and other network measures [38–40] have been used to characterize the structural changes in brain networks associated with epilepsy [41–44]. However, the variability introduced by thresholding and single-scale analyses can limit the reliability of these metrics [22,23]. Therefore, there is a need for methods that can construct robust functional brain networks by integrating multi-scale information.

In this paper, we propose a novel multi-scale information fusion (MSIF) framework for constructing brain networks from EEG data in epilepsy. This method integrates connectivity information across frequency bands, temporal scales, and functional network construction methods, providing a comprehensive representation of brain network dynamics that maximizes sensitivity to changes associated with seizures. By optimizing weight distributions through Particle Swarm Optimization (PSO), the framework adaptively focuses on the most informative connectivity patterns across epileptic states, improving the robustness and accuracy of network metrics.

We validate the proposed MSIF framework using EEG data from the CHB-MIT and Siena Epilepsy datasets, demonstrating its superior performance over traditional methods like wPLI, GC, and the Peter–Clark (PC) algorithm in distinguishing seizure and non-seizure states. The primary contributions of this study are:

1. Proposing a multi-scale information fusion framework that integrates connectivity data across frequency bands, temporal scales, and network construction methods, enabling comprehensive analysis of brain networks in epilepsy.
2. Introducing the Comprehensive Sensitivity Score (CSS) to evaluate the framework's performance, leveraging optimized weight distributions through PSO for robust detection of seizure-related network changes.
3. Validating the MSIF framework on clinical EEG datasets, demonstrating its superior performance over traditional methods in accurately distinguishing seizure states.

The remainder of this paper is structured as follows. In Section 1, we detail the MSIF framework's development and the associated optimization strategies for EEG-based network construction. Section 2 provides an extensive comparison of epilepsy states, including comprehensive analyses of network metrics. Finally, in Section 3, we explore the broader implications of these findings, discuss potential clinical applications, summarize the limitations of our work, and conclude with an outline of future research directions.

1. Multi-scale information fusion approach for brain network construction

The proposed multi-scale information fusion (MSIF) approach integrates multiple dimensions of EEG data analysis, combining information across frequency bands, temporal scales, and network construction methods. The framework starts with raw EEG data preprocessing, including steps such as bandpass filtering, noise removal, re-referencing, independent component analysis (ICA), and epoching. After preprocessing, the EEG signals are decomposed into different frequency bands (δ (0.5–4 Hz), θ (4–8 Hz), α (8–13 Hz), β (13–30 Hz), γ (30–100 Hz) [33]), segmented using multiple temporal windows (1-s, 5-s, and 10-s [45]), and analyzed with various network construction methods, including weighted phase lag index (wPLI), Granger causality (GC), and the Peter–Clark (PC) algorithm. Each frequency band contributes uniquely to the analysis of epileptic EEG signals. The delta and theta bands

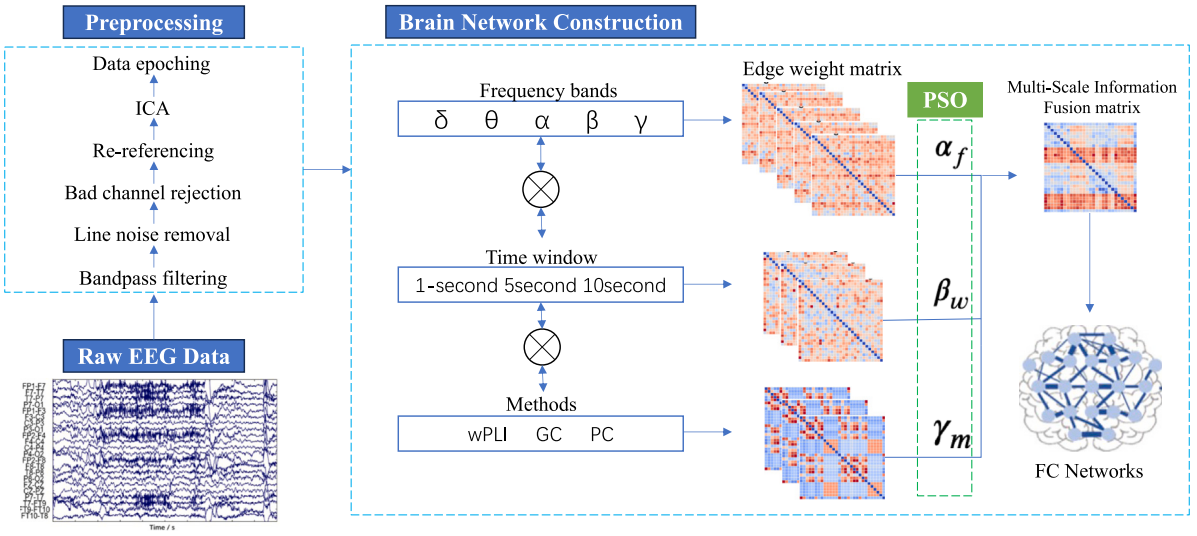

Fig. 1. Workflow of the multi-scale information fusion approach for brain network construction. The framework integrates preprocessing, brain network construction across multiple scales, and fusion of connectivity matrices using PSO.

often capture slow oscillations associated with cortical dysfunction and seizure precursors, respectively, while the alpha band reflects disrupted thalamocortical activity during seizures. The beta band is particularly relevant for identifying motor-related activity, and the gamma band highlights high-frequency neural synchronization during seizure onset. By integrating these distinct frequency-specific properties, the multi-scale framework effectively captures the complex dynamics of epileptic seizures across neural scales. The selection of these three methods—wPLI, Granger causality (GC), and the Peter–Clark (PC) algorithm—is driven by their complementary characteristics. wPLI is a widely used method for assessing phase synchronization and constructs symmetric connectivity networks, making it ideal for capturing global synchrony patterns [14]. GC focuses on linear causal relationships and generates asymmetric networks, providing insights into directional interactions between brain regions [15]. In contrast, the PC algorithm models nonlinear causal relationships in asymmetric networks, enabling the detection of more complex dependencies [16]. The combination of these approaches ensures a comprehensive analysis, capturing both symmetric and asymmetric, linear and nonlinear, synchronization and causal interactions within the brain network.

The resulting connectivity matrices are further processed using a multi-scale information fusion technique, which combines the connectivity information across these scales into a comprehensive fusion matrix. Particle Swarm Optimization (PSO) is applied to optimize the weights across dimensions, generating a fused connectivity matrix that is used to construct functional brain networks. This fusion method captures complex network interactions and enhances sensitivity to dynamic changes in network structure during seizure states. Fig. 1 illustrates the workflow of the proposed multi-scale information fusion approach.

Multi-frequency decomposition

EEG signals were decomposed into frequency bands to capture specific brain dynamics. Let $X_i(t)$ represent the time series for channel i. Each $X_i(t)$ was decomposed using wavelet transform or empirical mode decomposition (EMD) into frequency components:

$$X_i(t) = \sum_{f \in F} X_i^{(f)}(t), \tag{1}$$

where $F = \{\text{delta (0.5–4 Hz)}, \text{theta (4–8 Hz)}, \text{alpha (8–13 Hz)}, \text{beta (13–30 Hz)}, \text{gamma (30–100 Hz)}\}$. The component $X_i^{(f)}(t)$ corresponds to the signal at frequency f.

Sliding window segmentation

Each frequency component $X_i^{(f)}(t)$ was segmented using overlapping windows of various lengths. Let T represent the total recording duration and $w \in W$ denote window lengths (e.g., 1-second, 5-seconds and 10-seconds). Each window w is defined by:

$$X_i^{(f,w)}(t) = \{X_i^{(f)}(t) : t \in [t_0, t_0 + w], w \in W, t_0 \in [0, T - w]\}, \tag{2}$$

where t_0 is the window's start time. This segmentation captures both transient and sustained connectivity patterns.

Connectivity estimation across scales

For each window w and frequency f, connectivity between channels i and j was computed using multiple measures. Let $C_{ij}^{(m,f,w)}$ represent the connectivity measure m (e.g., wPLI, GC, and PC) for channels i and j in frequency f and window w:

$$C_{ij}^{(m,f,w)} = \text{Measure}(X_i^{(f,w)}, X_j^{(f,w)}), \tag{3}$$

This provided a comprehensive connectivity profile for each brain region pair.

Multi-scale information fusion

The multi-scale method combined connectivity data across frequencies, windows, and measures. For each channel pair (i, j), the fused connectivity C_{ij} was computed as:

$$C_{ij} = \sum_{f \in F} \alpha_f \sum_{w \in W} \beta_w \sum_{m \in M} \gamma_m \cdot C_{ij}^{(m,f,w)}, \tag{4}$$

where α_f, β_w, and γ_m are weights for frequency bands, window lengths, and connectivity measures, respectively. These weights were optimized to maximize seizure-phase discriminative power while ensuring stability in non-seizure states.

Optimization objectives

The optimization aimed to maximize the differences between seizure states, where I_k represents a network metric (e.g., global efficiency, clustering coefficient) computed for each state. Specifically, $I_k^{\text{pre-seizure}}$, I_k^{seizure}, and $I_k^{\text{post-seizure}}$ denote the average value of metric k during the pre-seizure, seizure, and post-seizure states, respectively.

The following optimization objectives were defined:

$$\begin{cases} \Delta I_k^{\text{pre-seizure}} = \left| \text{mean}(I_k^{\text{seizure}}) - \text{mean}(I_k^{\text{pre-seizure}}) \right|, \\ \Delta I_k^{\text{post-seizure}} = \left| \text{mean}(I_k^{\text{seizure}}) - \text{mean}(I_k^{\text{post-seizure}}) \right|, \\ \Delta I_k^{\text{pre-post}} = \left| \text{mean}(I_k^{\text{pre-seizure}}) - \text{mean}(I_k^{\text{post-seizure}}) \right|. \end{cases} \tag{5}$$

The objective function J was defined to maximize the discriminative power between seizure states while minimizing instability between non-seizure states:

$$J(\alpha_f, \beta_w, \gamma_m) = \max \sum_k \left(\Delta I_k^{\text{pre-seizure}} + \Delta I_k^{\text{post-seizure}} - \lambda \Delta I_k^{\text{pre-post}} \right), \tag{6}$$

where λ is a balancing parameter that ensures discriminative power is maximized while maintaining stability between non-seizure states. The weights α_f, β_w, and γ_m were optimized using Particle Swarm Optimization (PSO) to maximize J.

2. Experiment and results analysis

Data acquisition and preprocessing

EEG data for this study were obtained from two publicly available datasets: the CHB-MIT Scalp EEG Database[1] and the Siena Epilepsy Dataset[2]. These datasets were selected for their applicability in analyzing seizure dynamics and their inclusion of distinct seizure and non-seizure phases.

For the CHB-MIT dataset, we ensured consistency by selecting a standard set of 23 channels across all recordings and removing any additional channels. Data segments with fewer than 23 channels were excluded from analysis. Similarly, for the Siena dataset, 29 channels were consistently selected, with extra channels removed, and recordings with fewer than 29 channels were excluded. The preprocessing of EEG data involved several steps aimed at enhancing signal quality and ensuring uniformity. First, a band-pass filter (0.5–70 Hz) was applied to mitigate low-frequency drifts and high-frequency noise. Additionally, a notch filter at 60 Hz was used to eliminate power line noise, minimizing potential interference from electrical sources. Artifact removal was performed using Independent Component Analysis (ICA), effectively reducing non-neural components such as ocular and muscle artifacts. The EEG data were then re-referenced to an average reference to standardize signal interpretation across channels. The preprocessed EEG data were segmented into epochs corresponding to pre-seizure, seizure, and post-seizure states to facilitate targeted analysis. To ensure data consistency across recordings, z-score normalization was applied to each channel by calculating the mean and standard deviation, followed by standardizing the data. This step helped normalize the signal amplitude, enabling better comparison across different EEG segments and participants.

Our preprocessing approach drew inspiration from methodologies outlined in automated EEG processing pipelines, such as DISCOVER-EEG, which emphasizes robust, comprehensive preprocessing strategies for biomarker discovery in clinical neuroscience [46].

[1] https://physionet.org/content/chbmit/1.0.0/

[2] https://www.physionet.org/content/siena-scalp-eeg/1.0.0/

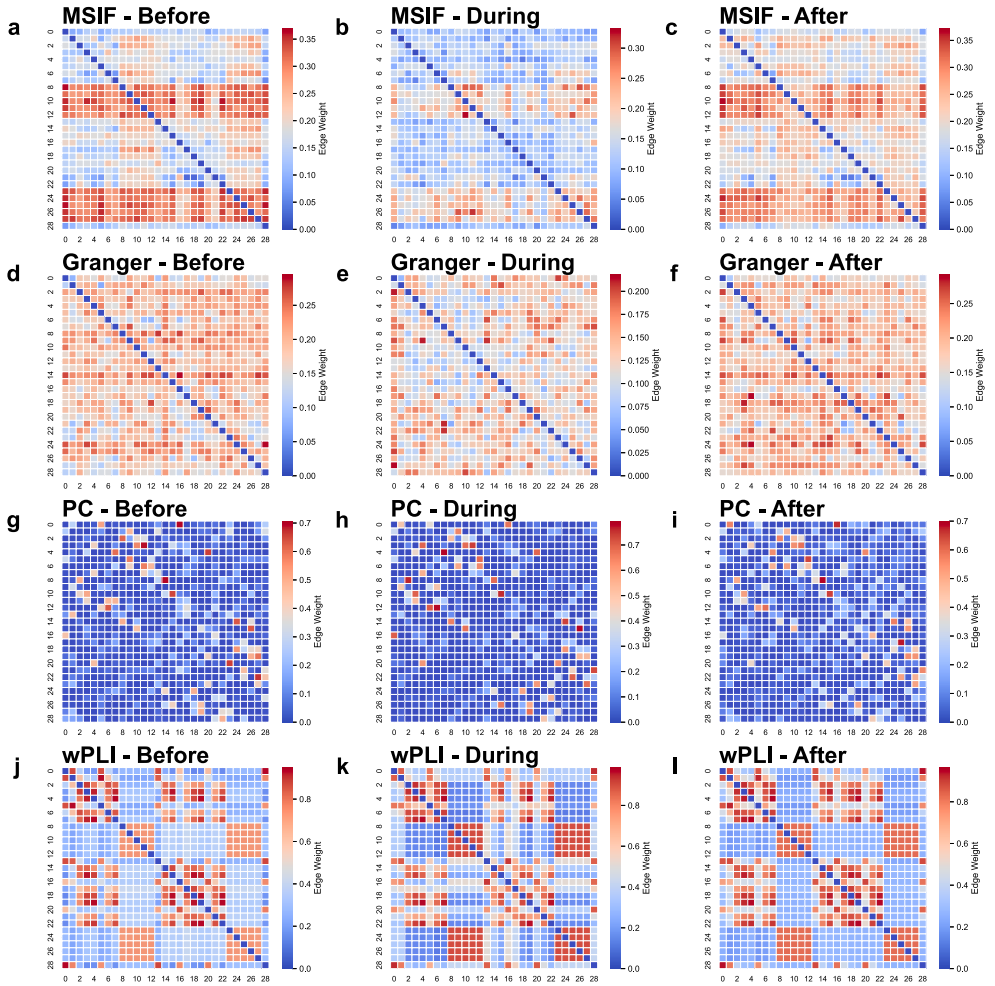

Fig. 2. Edge weight matrices constructed using different methods (MSIF, GC, PC and wPLI) across pre-seizure, seizure, and post-seizure states from the Siena dataset. Red hues represent higher connectivity strengths, whereas blue hues indicate weaker or inhibitory connections.

Comparison of edge weight matrices and networks constructed using different methods

To evaluate the effectiveness of different brain network construction methods in distinguishing seizure dynamics, we compared the performance of our proposed multi-scale information fusion approach against three traditional connectivity estimation methods: weighted phase lag index (wPLI), Granger causality (GC), and the Peter–Clark (PC) algorithm. Each method's results are analyzed across three temporal stages—pre-seizure, seizure, and post-seizure—using both connectivity matrices (Fig. 2) and circular network diagrams (Fig. 3).

The comparative analysis of different network construction methods reveals notable differences in their ability to capture and differentiate the dynamic shifts associated with seizure activity. Our proposed multi-scale information fusion (MSIF) method stands out due to its comprehensive approach, effectively highlighting distinct connectivity changes across the pre-seizure, seizure, and post-seizure phases (Fig. 2a-c and Fig. 3a-c). We can see that, compared to other methods, the matrices and circular diagrams obtained using our MSIF method show the closest similarity between the pre-seizure and post-seizure phases, while exhibiting the largest differences between the pre-seizure/post-seizure phases and the seizure phase. Unlike traditional methods, MSIF captures nuanced temporal and frequency-specific variations, providing a more detailed representation of the underlying network dynamics.

The matrix comparison results further substantiate these observations, as shown in Table 1, which lists the Mean Squared Error (MSE) and Frobenius Norm between connectivity matrices across the three stages (Before vs During, Before vs After, During vs After), along with the percentage changes relative to the "Before & After" values. MSIF achieves the lowest MSE in the "Before & After" comparison (0.00132), indicating that the network connectivity returns closer to its baseline state post-seizure. Simultaneously, it exhibits the highest percentage changes in MSE for the "Before & During" (603.03%) and "During & After" (618.94%) comparisons, reflecting its superior sensitivity to seizure-induced disruptions.

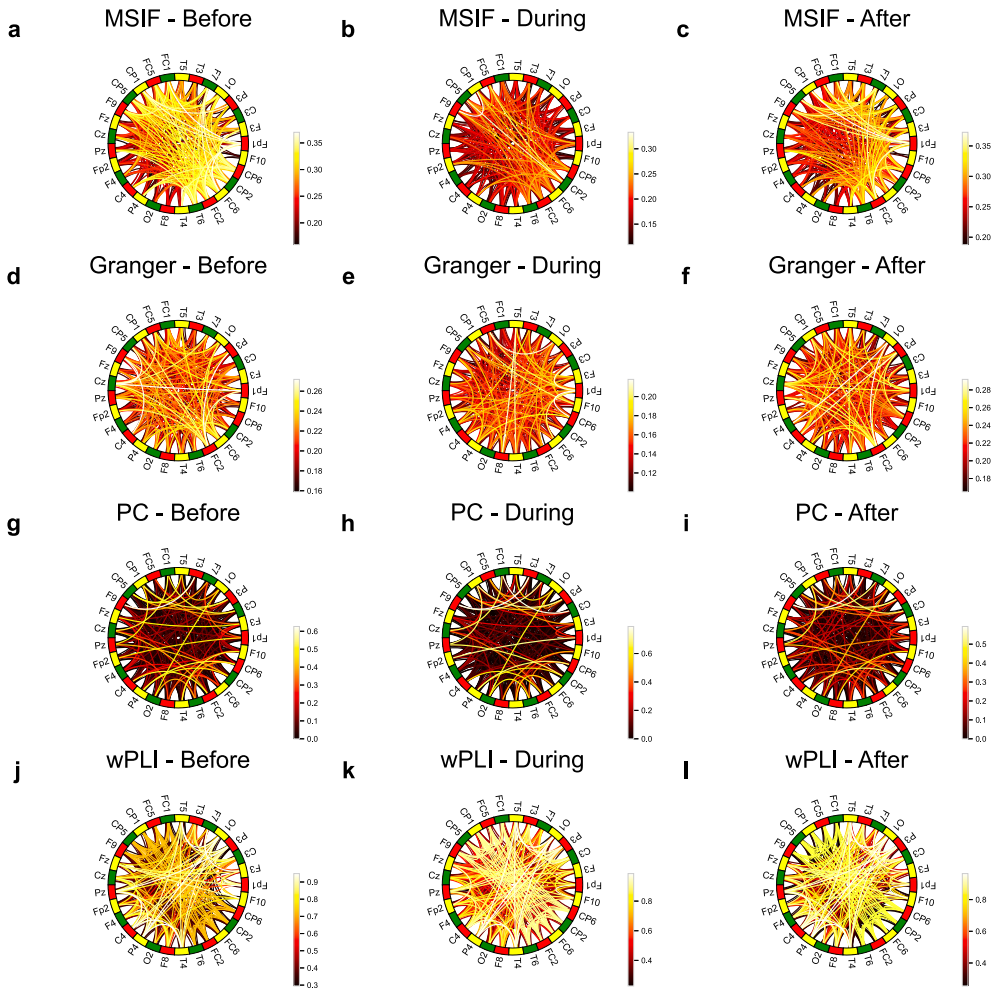

Fig. 3. Circular network representations of brain connectivity using different methods (MSIF, wPLI, GC, and PC) across pre-seizure, seizure, and post-seizure states from the Siena dataset. The color intensity and thickness of connections represent the edge weights, highlighting connectivity strengths.

Similarly, the Frobenius Norm for MSIF is lowest in the "Before & After" comparison (1.0546), and shows the largest percentage increases in the "Before & During" (245.34%) and "During & After" (248.53%) comparisons. This pattern demonstrates that MSIF not only captures significant alterations in network connectivity during seizures but also effectively represents the recovery to baseline connectivity post-seizure. The higher sensitivity of MSIF to these transitions is also evident in its ability to capture detailed patterns in circular diagrams (Fig. 3a-c), where seizure-related synchronizations (Fig. 3b) are significantly different compared to the pre- and post-seizure phases (Fig. 3a,c).

The Granger causality (GC) method demonstrates a certain level of sensitivity in identifying seizure-related network changes, as evidenced by its intermediate MSE percentage changes (380.00% for "Before & During") and Frobenius Norm percentage changes (195.05% for "Before & During"). However, when compared to our proposed MSIF method, GC shows inferior performance, with lower percentage changes in both MSE and Frobenius Norm during seizure transitions, indicating reduced sensitivity to seizure-induced disruptions. Additionally, the higher MSE in the "Before & After" comparison (0.00150) suggests slightly reduced precision in capturing the recovery to baseline connectivity post-seizure. The circular diagrams for GC (Fig. 3d-f) show some differences across seizure phases, but the changes are less pronounced than those observed with MSIF.

The Peter–Clark (PC) algorithm exhibits limited sensitivity across all comparisons, with the lowest percentage changes in MSE (121.20% for "Before & During") and Frobenius Norm (110.10% for "Before & During"). The higher MSE in the "Before & After" comparison (0.00415) further highlights the algorithm's reduced capacity to capture subtle network changes. The circular diagrams generated by the PC algorithm are sparse and fragmented (Fig. 3g-i), failing to illustrate the significant synchrony differences observed during seizures.

The weighted phase lag index (wPLI) method exhibits the highest MSE and Frobenius Norm values across all comparisons. Although it shows moderate percentage changes in MSE (260.52% for "Before & During"), the higher baseline MSE in the "Before

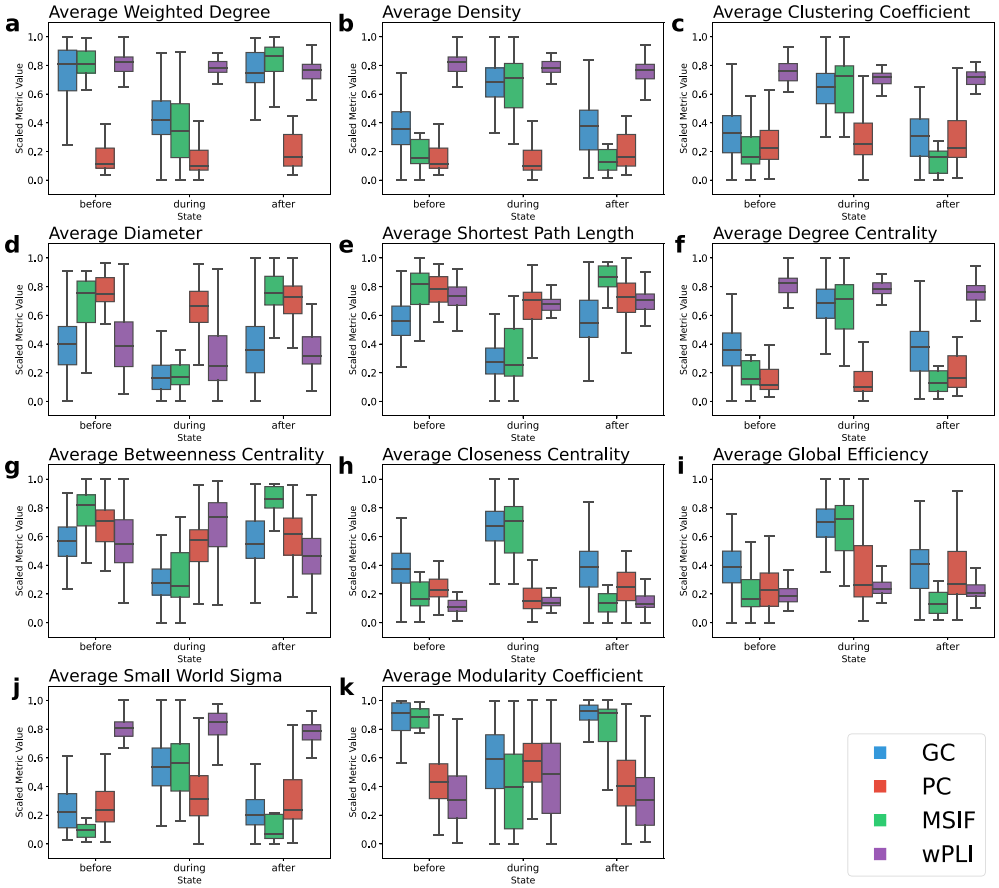

Fig. 4. Box plot comparison of network metrics across different methods (Granger causality (GC), PC algorithm, proposed multi-scale information fusion method (MSIF), and wPLI) for pre-seizure, seizure, and post-seizure phases from the Siena dataset. Each box plot represents the distribution of metric values across multiple patient samples, showing the variability within each seizure stage. The proposed multi-scale method exhibits the most pronounced separation between seizure and non-seizure states, with concentrated distributions within most stage, indicating higher robustness.

Table 1
Comparison of Connectivity Matrices for Different Methods Across Seizure Phases with Percentage Changes. A model is considered better if the "Before & After" MSE and Frobenius Norm values are smaller, indicating better recovery to baseline connectivity, while the percentage changes for "Before & During" and "During & After" are larger, reflecting the model's sensitivity to seizure-induced disruptions. The percentage change columns represent the MSE and Frobenius Norm relative to the "Before & After" values within the same method.

Method	Comparison	MSE	MSE change (%)	Frobenius norm	Frobenius norm change (%)
MSIF	Before & During	0.00796	**603.03**	2.58734	**245.34**
	Before & After	**0.00132**	/	**1.05460**	/
	During & After	0.00817	**618.94**	2.62099	**248.53**
Granger	Before & During	0.00570	380.00	2.18969	195.05
	Before & After	0.00150	/	1.12263	/
	During & After	0.00557	371.33	2.16436	192.75
PC	Before & During	0.00503	121.20	2.05703	110.10
	Before & After	0.00415	/	1.86762	/
	During & After	0.00543	130.84	2.13692	114.43
wPLI	Before & During	0.01920	260.52	4.01878	161.42
	Before & After	0.00737	/	2.48997	/
	During & After	0.01211	164.29	3.19148	128.20

& After" comparison (0.00737) indicates weaker robustness in identifying non-seizure states. Additionally, the minimal differences observed in wPLI's circular diagrams (Fig. 3j-l) further highlight its limitations in capturing global and inter-regional connectivity changes.

In conclusion, the MSIF method consistently outperforms traditional approaches in detecting seizure-induced changes while effectively distinguishing between pre-seizure, seizure, and post-seizure states. Its superior performance in terms of both absolute values and percentage changes of MSE and Frobenius Norm, along with the clear visual differentiation observed in the matrix

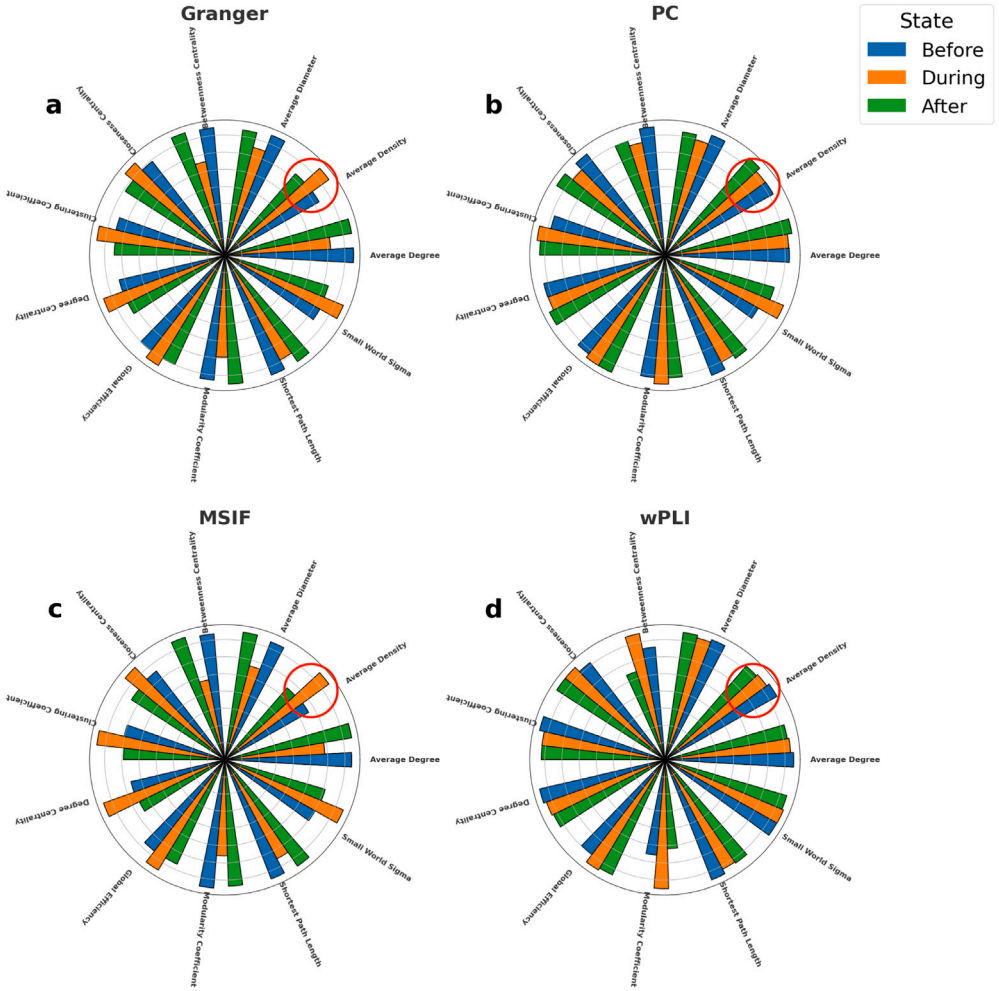

Fig. 5. Comparison of average network metrics across different methods (GC, PC, our proposed multi-scale information fusion method (MSIF), and wPLI) for pre-seizure, seizure, and post-seizure phases. Each bar represents the value of specific network metrics across the three stages. The performance is better when the orange bar (during seizure) differs more significantly from the blue and green bars (before and after seizure) while the blue and green bars (before and after seizure) show minimal differences from each other. The proposed multi-scale method (c) shows the most pronounced differences between the phases, indicating its superior ability to capture dynamic changes in network structure during seizures compared to other methods.

(Fig. 2a-c) and circular diagram comparisons (Fig. 3a-c), underscores its potential in developing network-based biomarkers for epilepsy diagnosis and monitoring.

Network metric analysis across methods and states

To assess the capability of each method in capturing network characteristics across pre-seizure, seizure, and post-seizure states, we conducted a detailed analysis of network metrics, including centrality, small-world index and other related network measures, using patient-wise distributions (Fig. 4) and normalized data representations (Fig. 5). These metrics were chosen based on their widespread use in prior studies for characterizing brain network dynamics in epilepsy [41–44] and their ability to provide a comprehensive assessment of network properties, covering aspects such as connectivity strength, efficiency, centrality, and modularity, which are crucial for understanding both global and local network changes during different seizure states. These visualizations provide insights into the performance of each method, emphasizing the effectiveness of our multi-scale information fusion approach in detecting state-specific connectivity changes associated with epilepsy.

Patient-wise metric distribution. Our proposed multi-scale information fusion method exhibits superior performance in distinguishing seizure (during) from non-seizure (pre-seizure and post-seizure) states, as demonstrated by its ability to create the most pronounced separation between these phases and maintain concentrated distributions for each phase (Fig. 4). The reduced variability within each seizure stage, reflected by narrower interquartile ranges (IQRs), indicates better robustness and consistency in detecting

patient-specific seizure dynamics. This is particularly evident in metrics (Fig. 4b,d,f), where the seizure phase shows a significant deviation from non-seizure phases, with pre-seizure and post-seizure values being closely aligned, highlighting effective recovery representation.

The Granger causality method shows reasonable performance in distinguishing between seizure and non-seizure states, with noticeable shifts in median values across phases (*average degree centrality* in Fig. 4f). However, compared to our proposed multi-scale information fusion method, Granger causality exhibits less concentration in data distribution within each phase and a lower degree of differentiation between the seizure phase and non-seizure phases(Fig. 4b). This suggests that while Granger causality can capture some network changes associated with seizures, it falls short in terms of robustness and precision.

The PC algorithm shows significant limitations, displaying minimal variability across seizure stages and broad distributions indicating high inter-patient variability (e.g., *average diameter* in Fig. 4d and *average closeness centrality* in Fig. 4h). The subtle shifts in median values suggest that the PC algorithm is not effective at capturing dynamic changes during seizures, likely due to its reliance on strict conditional independence assumptions, which can lead to underestimation of connectivity during highly synchronized states.

The wPLI method also demonstrates limited performance, often failing to effectively differentiate between seizure and non-seizure states across various metrics, such as *small world sigma* (Fig. 4j). While wPLI can identify certain seizure-related changes, its broader IQRs and overlapping distributions for pre-seizure and post-seizure phases indicate a reduced ability to consistently and accurately represent transitions between these states.

Average network metrics across methods. The comparison of network metrics across different methods highlights notable differences in their ability to capture changes between the pre-seizure, seizure, and post-seizure states. Fig. 5 provides a comprehensive view of the relative performance of Granger causality (a), the Peter–Clark (PC) algorithm (b), our proposed multi-scale information fusion method (c), and the weighted phase lag index (wPLI) (d).

The Granger causality method (Fig. 5a) shows some distinction between the seizure and non-seizure phases. However, the changes across nearly all network metrics are less pronounced compared to those observed in the MSIF method (as highlighted by the red circles in Fig. 5a-d). This indicates that while Granger causality can detect shifts in network structure, it lacks sufficient sensitivity to capture the significance of these changes. This limitation is evident from the relatively uniform bar heights across the different phases.

The PC algorithm (Fig. 5b) demonstrates minimal differences across the pre-seizure, seizure, and post-seizure phases. Most network metrics, including path length and modularity, show very slight variations, indicating that the PC algorithm may underestimate connectivity, especially during highly synchronized seizure events. This results in a limited ability to reveal substantial differences between stages.

The wPLI method (Fig. 5d) exhibits moderate changes across different seizure stages, with certain metrics (such as modularity and betweenness centrality) showing higher values during seizures compared to non-seizure phases. However, for most metrics, the differences between the pre-seizure, seizure, and post-seizure stages are less pronounced. This indicates that while wPLI demonstrates a certain sensitivity to localized synchrony, it may fail to effectively capture the more subtle network changes associated with seizure activity.

In contrast, our proposed multi-scale information fusion method (Fig. 5c) demonstrates the most significant differences between the seizure and none-seizure phases across nearly all network metrics. Metrics such as global efficiency, betweenness centrality, and small-world sigma show substantial increases during the seizure phase, with clear reductions post-seizure, indicating a partial return to baseline. This distinct separation across stages suggests that our multi-scale method captures the complex, multi-dimensional nature of seizure dynamics more effectively than the other methods. The greater variability in bar heights reflects the method's capacity to integrate diverse scales of information, providing a more detailed and comprehensive view of brain network changes associated with epilepsy.

Overall, the proposed multi-scale approach outperforms the traditional methods by demonstrating greater sensitivity to network changes during seizures and providing clear distinctions between the different seizure states.

Optimization of multi-scale weights

To improve the performance of our multi-scale information fusion method in detecting and distinguishing seizure dynamics, we applied Particle Swarm Optimization (PSO) to optimize the weights assigned to each frequency band, time window, and connectivity measure. The PSO algorithm parameters were carefully selected to achieve stable convergence while balancing computational efficiency. We set the minimum weight resolution increment to 0.02, a choice driven by computational constraints that balances precision with practicality, allowing the algorithm to reach a global or near-global optimum within a feasible timeframe. The PSO algorithm was configured with the parameters shown in Table C.1, providing a balance between convergence stability and computational efficiency. These settings were applied to both the CHB-MIT and Siena datasets.

Following PSO optimization, we obtained two distinct sets of weight parameters tailored for the CHB-MIT and Siena datasets, as shown in Tables 2 and D.1. The differences in weights reflect dataset-specific characteristics, with adjustments that account for variations in signal properties and seizure dynamics between the two datasets.

The optimized weights for the CHB-MIT and Siena datasets reveal significant differences, particularly in their distribution across frequency bands and time windows, which align with the electrode configurations used in these datasets. Notably, these differences also reflect the distinct physiological roles of each frequency band in epileptic EEG. In the literature, delta (0.5–4 Hz) and theta

Table 2
Optimized Weights for Frequency Bands, Time Windows, and Connectivity Measures for the Siena Dataset.

Weight type	Parameter	Weight value
Frequency Band Weights (α_f)	Delta (0.5–4 Hz)	$\alpha_{\text{delta}} = 0.34$
	Theta (4–8 Hz)	$\alpha_{\text{theta}} = 0.26$
	Alpha (8–13 Hz)	$\alpha_{\text{alpha}} = 0.12$
	Beta (13–30 Hz)	$\alpha_{\text{beta}} = 0.14$
	Gamma (30–100 Hz)	$\alpha_{\text{gamma}} = 0.14$
Time Window Length Weights (β_{tw})	1-second window	$\beta_{1s} = 0.12$
	5-second window	$\beta_{5s} = 0.24$
	10-second window	$\beta_{10s} = 0.64$
Connectivity Measure Weights (γ_m)	Weighted Phase Lag Index (wPLI)	$\gamma_{\text{wPLI}} = 0.16$
	Granger Causality (GC)	$\gamma_{\text{GC}} = 0.62$
	Peter–Clark (PC)	$\gamma_{\text{PC}} = 0.22$

(4–8 Hz) bands have often been linked to broad or global cortical slowing, which can signal pathological synchronization and seizure onset; alpha (8–13 Hz) and beta (13–30 Hz) bands frequently index resting-state activities and motor-related functions, respectively; and gamma (30–100 Hz) is commonly associated with fast oscillations, playing a key role in local, high-frequency discharges often implicated in epileptogenic regions [17].

In the case of the CHB-MIT dataset (Table D.1), which utilizes bipolar electrode placement to emphasize local brain region activities, the method assigns relatively higher weights to the beta ($\alpha_{\text{beta}} = 0.22$) and gamma ($\alpha_{\text{gamma}} = 0.38$) frequency bands. These findings support the importance of high-frequency components for capturing focal epileptic signatures and localized neuronal bursts [47,48]. Additionally, the stronger preference for the 5-second ($\beta_{5s} = 0.56$) time window further underscores the advantage of bipolar electrodes in revealing short-term, localized network dynamics related to rapid seizure onset.

By contrast, the Siena dataset (Table 2) employs monopolar electrode placement, which is better suited for recording broader, longer-lasting global effects. Accordingly, the optimization favors lower frequency bands, such as delta ($\alpha_{\text{delta}} = 0.34$) and theta ($\alpha_{\text{theta}} = 0.26$), well-known for capturing large-scale synchronies and slow oscillatory activity often characteristic of diffuse seizure propagation. The higher weight assigned to the 10-second time window ($\beta_{10s} = 0.64$) similarly reflects the method's ability to track more global, sustained network states in monopolar recordings over extended periods. This is consistent with the notion that, in generalized seizures, lower-frequency rhythmic patterns and prolonged network involvement are more relevant to understanding overall cortical excitability.

These parameter optimizations reflect the inherent differences in the CHB-MIT and Siena datasets and the electrode configurations that guide their analysis. The CHB-MIT dataset benefits from a focus on high-frequency bands and shorter time windows to capture rapid, localized brain activity characteristic of bipolar recordings [49]. Conversely, the Siena dataset prioritizes lower frequency bands and longer time windows, aligning with the strengths of monopolar recordings in capturing global, long-term brain connectivity [50].

The choice of a 0.02 increment resolution for weight adjustments ensures a balance between computational efficiency and precision in parameter tuning. This granularity allows the PSO algorithm to make refined adjustments without incurring high computational costs. Ensuring that the weights sum to 1 within each category (frequency band, time window, connectivity measure) maintains model stability, preventing over-reliance on any single parameter and promoting balanced contributions from all components.

Statistical analysis of network construction methods: Comparative performance

To evaluate the effectiveness of each network construction method, we conducted paired t-tests on network metrics across different seizure states (Before vs During, Before vs After, and During vs After) for the Siena dataset. The p-values for each metric are summarized in Tables 3, A.1, and A.2, and are visualized in Fig. 6. The multi-scale information fusion(MSIF) approach consistently achieves low p-values in 'Before vs During' and 'During vs After' comparisons and higher p-values in 'Before vs After' comparisons, demonstrating its superior ability to distinguish seizure-related network changes.

The comparative performance of the network construction methods, as assessed through statistical analysis of p-values for different seizure state comparisons (Tables 3, A.1, and A.2), reveals notable insights. The multi-scale information fusion(MSIF) approach consistently achieves low p-values in the 'Before vs During' and 'During vs After' comparisons, indicating high sensitivity to the initial changes in network dynamics at seizure onset and the reorganization of connectivity post-seizure. Metrics such as Average Density, Average Clustering Coefficient, and Average Global Efficiency show significant p-values well below the 0.05 threshold, confirming the method's efficacy in detecting seizure-related connectivity disruptions. The desired *inverted V-shaped pattern* in Fig. 6 supports these findings, with low p-values for the 'Before vs During' and 'During vs After' comparisons and higher p-values for the 'Before vs After' comparison. This pattern demonstrates that the multi-scale information fusion(MSIF) approach not only captures seizure-induced changes but also accurately identifies the stability between pre-seizure and post-seizure states.

In contrast, the Granger causality method shows reasonable performance with significant p-values in the 'Before vs During' and 'During vs After' comparisons, reflecting its ability to identify changes during seizures. However, it falls short in terms of data distribution concentration and differentiation between pre-seizure and post-seizure states when compared to the multi-scale

Table 3
p-values for Network Metrics: Before vs During (Siena Dataset). The bold values represent the smallest *p*-value for each metric, while the values marked with † indicate the second smallest *p*-value for each metric.

Network metric	**wPLI**	GC	PC	MSIF
Average Weighted Degree Coefficient	0.2495	**0.0036**	0.0792	0.0071†
Average Density	0.2495	0.0104†	0.0792	**0.0028**
Average Clustering Coefficient	0.2324	0.0125†	0.4749	**0.0040**
Average Diameter	0.9322	0.0438†	0.2794	**0.0136**
Average Shortest Path Length	0.8689	0.0112†	0.5367	**0.0030**
Average Degree Centrality	0.7642	0.0632†	0.5238	**0.0228**
Average Betweenness Centrality	0.8324	0.1274†	0.6587	**0.0534**
Average Closeness Centrality	0.6743	0.0845†	0.7463	**0.0230**
Average Global Efficiency	0.7316	0.0234†	0.7486	**0.0030**
Average Small World Sigma	0.8023	0.0917†	0.7214	**0.0314**
Average Modularity Coefficient	0.6283	0.1176†	0.8253	**0.0616**

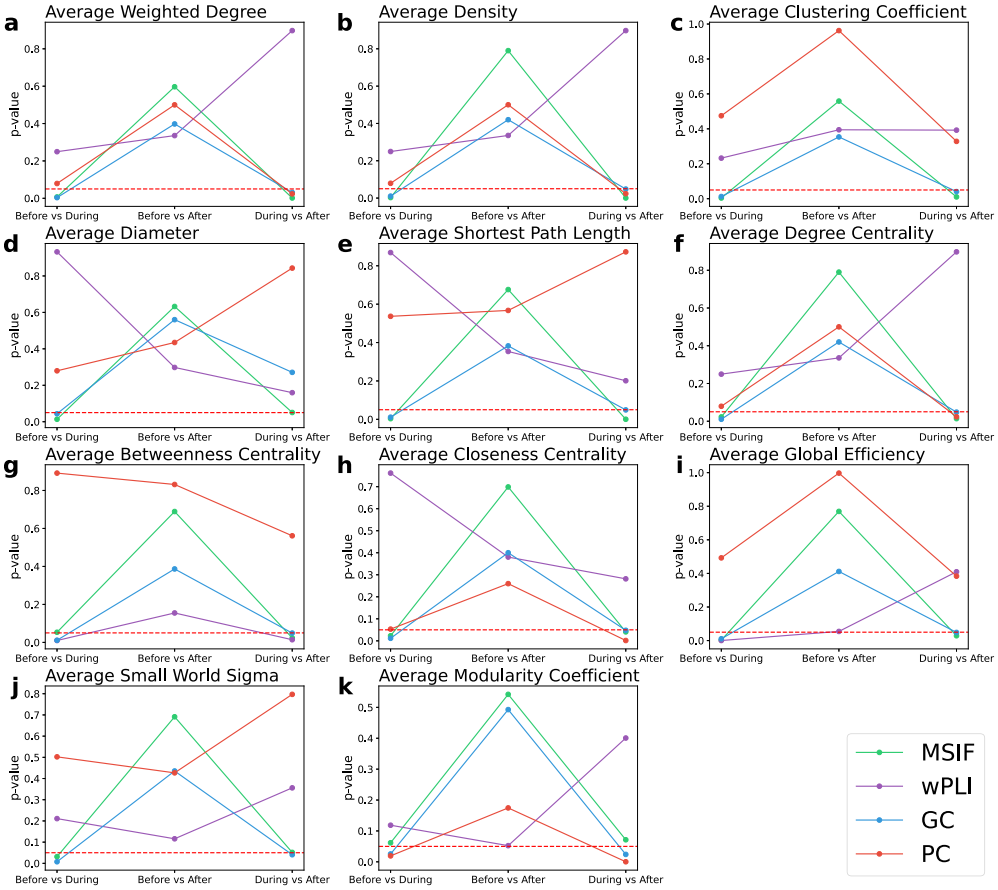

Fig. 6. P-values for different network metrics across methods (Ours, wPLI, Granger, PC) in 'Before vs During', 'Before vs After', and 'During vs After' comparisons using the Siena Dataset. For each metric, the ideal trend is to observe an *inverted V-shaped pattern*, characterized by lower p-values in 'Before vs During' and 'During vs After' comparisons and higher p-values in 'Before vs After'. This pattern indicates that a method effectively captures significant network changes associated with seizure events, while recognizing the stability between pre-seizure and post-seizure states. The red dashed line indicates the significance threshold ($p = 0.05$).

information fusion(MSIF) method. The PC algorithm and wPLI method, meanwhile, exhibit greater limitations. Both methods often display higher p-values or inconsistent trends, indicating reduced sensitivity to seizure transitions and a lack of clear differentiation between seizure and non-seizure states. This is particularly evident in their performance for key metrics such as Average Shortest Path Length (Fig. 6e) and Average Small World Sigma(Fig. 6j), where the p-values are not consistently significant across phases.

The analysis underscores that while Granger causality shows moderate effectiveness, the PC algorithm and wPLI method struggle to differentiate between phases with the same level of precision. The multi-scale information fusion(MSIF) method outperforms these

Table 4
Comprehensive Sensitivity Score (CSS) for Network Construction Methods (Siena and CHB-MIT Datasets).

Method	CSS value (Siena)	CSS value (CHB-MIT)
Multi-Scale Information Fusion (MSIF)	**2.8879**	**2.3518**
Granger Causality (GC)	2.1063	1.0458
Peter–Clark (PC)	1.4191	1.1718
weighted phase lag index (wPLI)	0.7812	1.9204

traditional methods, demonstrating superior robustness in identifying seizure-related network changes and maintaining stability across pre- and post-seizure states, as highlighted by its consistent *inverted V-shaped pattern* in p-value trends.

Scoring analysis of network construction methods: Comprehensive sensitivity score (CSS)

Paired t-tests were conducted to evaluate the significance of network metric differences between seizure states (Before vs During, During vs After, and Before vs After). P-values (p_1, p_2, and p_3) were computed for each metric to identify statistically significant changes. The Comprehensive Sensitivity Score (CSS) was calculated using these p-values and optimized weights to quantify the discriminative performance of each method. As defined in Eq. (7), the CSS incorporates weights w_1, w_2, and w_3 for each p-value, penalty coefficients α and β, and an indicator function $I(\cdot)$ to account for specific conditions. The term γ emphasizes variation between p-values to encourage more distinct phase separations. This comprehensive approach quantifies the sensitivity and stability of network metrics across seizure states.

To quantitatively assess the performance of each network construction method, we developed the Comprehensive Sensitivity Score (CSS), calculated using the following formula:

$$\begin{aligned} CSS = 1 &- w_1 \cdot (p_1 + \alpha \cdot I(p_1 > 0.05)) - w_2 \cdot (p_2 + \alpha \cdot I(p_2 > 0.05)) \\ &+ w_3 \cdot (p_3 - \beta \cdot I(p_3 < 0.05)) + \gamma \cdot (|p_1 - p_3| + |p_2 - p_3|). \end{aligned} \tag{7}$$

Table in Appendix B explains the parameters used in the CSS formula. The CSS formula is designed to capture both the discriminative power and stability of network metrics across seizure states. Below, we provide a detailed explanation of the rationale for each component:

1. **Weights** w_1, w_2, w_3: Each weight corresponds to a specific comparison: w_1 for "Before vs During," w_2 for "During vs After," and w_3 for "Before vs After." These weights allow the formula to prioritize the importance of each comparison based on the context of the analysis. For example, larger weights for w_1 and w_2 emphasize sensitivity to seizure-induced changes, while w_3 ensures stability between pre- and post-seizure states.
2. **Penalty Coefficients** α and β: Penalties are applied to encourage statistically significant results. α penalizes p-values greater than 0.05 in p_1 and p_2, ensuring that the method is sensitive to changes during and immediately after the seizure. Conversely, β penalizes p-values below 0.05 in p_3, promoting stability between pre-seizure and post-seizure states.
3. **Indicator Function** $I(\cdot)$: The indicator function $I(\text{p}> 0.05)$ and $I(\text{p}< 0.05)$ ensures that penalties are applied only when specific conditions are met. This prevents unnecessary penalization and focuses the score on meaningful statistical thresholds.
4. **Variation Term** $\gamma \cdot (|p_1 - p_3| + |p_2 - p_3|)$: This term emphasizes the importance of variation between the phases. By encouraging larger differences between p_1, p_2 (related to seizure phases) and p_3 (non-seizure phases), the formula ensures that the score reflects the method's ability to distinguish seizure-related transitions.

Consider a method where p_1 and p_2 are significantly below 0.05, indicating high sensitivity to seizure transitions, while p_3 is above 0.05, demonstrating stability between pre- and post-seizure states. For such a case, the CSS would yield a high score due to minimal penalties and substantial phase separations. Conversely, a method with inconsistent or insignificant p-values (e.g., $p_1, p_2 > 0.05$) would receive a lower score due to increased penalties and reduced variation between phases. This comprehensive scoring framework ensures that the CSS captures the dual requirements of sensitivity to seizure-induced changes and stability in non-seizure states, making it a robust metric for evaluating network construction methods.

For both the Siena and CHB-MIT datasets, the multi-scale information fusion (MSIF) method consistently achieved the highest CSS, indicating its superior ability to capture significant seizure-related changes while maintaining network stability between pre- and post-seizure states. Table 4 summarizes the CSS values for each network construction method across both datasets.

The results in Tables 4 highlight the overall advantage of the multi-scale information fusion (MSIF) approach across different datasets, providing comprehensive and reliable detection of complex network dynamics associated with seizures. The method's higher CSS values demonstrate its potential as a robust tool for developing network-based biomarkers in epilepsy diagnosis and monitoring.

3. Discussion and conclusion

This study introduces a novel multi-scale information fusion (MSIF) framework for constructing brain networks from EEG data in epilepsy analysis. By integrating connectivity information across multiple frequency bands, temporal scales, and network construction methods, the proposed approach addresses the limitations of traditional single-scale techniques such as Granger

causality (GC), the Peter–Clark (PC) algorithm, and the weighted phase lag index (wPLI). The MSIF framework demonstrates its capacity to capture complex, multi-dimensional network dynamics that are fundamental to understanding epileptic seizures and their associated brain activity, offering a significant advancement over conventional methods in the field.

The superior performance of the MSIF method, as demonstrated in both the CHB-MIT and Siena epilepsy datasets, highlights its ability to distinguish between seizure and non-seizure states with higher sensitivity and accuracy. This is primarily attributed to the framework's adaptive integration of multi-scale information, which allows for a more nuanced representation of the brain's connectivity dynamics during different stages of the seizure cycle. The results show that MSIF effectively captures intricate temporal and frequency-specific changes, enabling a more accurate characterization of brain networks during seizure events and recovery phases.

The adaptability of MSIF to different EEG recording configurations, such as bipolar and monopolar electrode setups, further underscores its versatility. By using Particle Swarm Optimization (PSO) to optimize the weights assigned to frequency bands, time windows, and connectivity measures, MSIF can tailor its analysis to dataset-specific characteristics. For instance, in the CHB-MIT dataset, the method places greater emphasis on higher-frequency bands and shorter time windows, capturing rapid, localized changes typical of focal seizures. Conversely, the Siena dataset, which uses monopolar electrode configurations, benefits from a focus on lower-frequency bands and longer time windows, suited for analyzing more widespread and sustained brain connectivity patterns. This flexibility makes the MSIF framework adaptable to diverse clinical settings, enhancing its potential as a diagnostic tool.

The implications of our findings extend beyond the immediate results. Our ability to detect seizure-related brain network changes aligns with growing neuroscientific theories regarding the hierarchical organization of epileptic networks. Specifically, seizures are often thought to originate from localized pathological hyper-synchronizations, which may then spread to larger brain regions, disrupting global brain connectivity [51]. Our framework, by revealing multi-scale disruptions, adds weight to this hypothesis and provides evidence that epileptic seizures involve not only local network disturbances but also large-scale reconfigurations. The high-frequency connectivity shifts observed in our study are particularly relevant to the concept of excitatory–inhibitory imbalance in epilepsy, which has been proposed as a driving force for seizure initiation and propagation [52]. Moreover, the MSIF framework's ability to identify pre-seizure network alterations may offer new insights into the transition from interictal to ictal states, contributing to ongoing debates on the predictability of seizures. By capturing subtle pre-seizure changes, the MSIF method supports the idea that brain networks undergo reconfigurations before the onset of overt seizure activity, which could eventually lead to more effective seizure prediction and early intervention strategies.

Our findings also have clinical implications, particularly in the development of seizure prediction systems. The MSIF framework's ability to robustly differentiate between pre-seizure, seizure, and post-seizure states may enable earlier identification of seizures, allowing clinicians to intervene before the full onset of a seizure. This could significantly improve patient outcomes by enabling timely pharmacological or neuromodulatory interventions. Furthermore, the integration of multi-scale information in brain network analysis suggests a new direction for developing personalized therapeutic strategies, such as tailored neurostimulation protocols or individualized medication plans based on dynamic changes in brain connectivity.

Despite its promising performance, there are several limitations to the MSIF method that need to be addressed in future research. One of the primary limitations is the lack of real-time implementation. Currently, the method operates in an offline mode, which limits its potential for clinical application where real-time seizure detection and prediction are crucial. The development of a real-time version of MSIF would enable continuous monitoring of brain activity and provide instant feedback, which is essential for clinical decision-making in epilepsy care. Additionally, although the CHB-MIT and Siena datasets provide valuable insights, they are limited in terms of sample size and diversity. Future research should focus on validating the MSIF framework on larger, more diverse datasets, including those that cover different types of epilepsy and patient populations. This would improve the generalizability of the findings and enhance the robustness of the method in real-world clinical settings. Furthermore, while MSIF provides a more comprehensive view of brain network dynamics, translating these findings into clinically actionable insights remains a challenge. Further collaboration with neurologists and clinicians is necessary to bridge the gap between network analysis and practical therapeutic applications.

Moreover, exploring aperiodic components in EEG signals for epilepsy analysis holds significant value. Existing studies suggest that alterations in 1/f-like power spectrum slopes can provide supplementary biomarkers for multiple neurological conditions. For instance, Yu et al. [53] demonstrated that aperiodic components, such as the 1/f-like slope and offset, reflect meaningful neurophysiological processes, including the excitatory–inhibitory (E/I) balance and regional brain sensitivities, which are modulated during acupuncture stimulation. Similarly, Yu et al. [54] highlighted the dynamic interplay between periodic alpha power and aperiodic slope during peripheral nerve stimulation, showing that these parameters can serve as effective biomarkers to decode brain responses and characterize neural entrainment. Incorporating these analyses may further enhance sensitivity to subtle changes in brain networks, especially those not captured by traditional periodic indicators during epileptic seizures.

In conclusion, the proposed MSIF framework offers a powerful, flexible, and scalable approach for analyzing brain network dynamics in epilepsy. Its ability to integrate connectivity information across multiple scales and its demonstrated superiority in capturing seizure-related changes position it as a promising tool for both research and clinical applications. Moving forward, we plan to expand the framework by incorporating real-time processing, integrating multimodal data, and investigating aperiodic EEG components to further enhance its clinical applicability. These advancements will pave the way for more accurate seizure prediction systems and personalized treatment approaches, ultimately improving the quality of care for patients with epilepsy.

CRediT authorship contribution statement

Zhiwen Ren: Writing – review & editing, Writing – original draft, Visualization, Validation, Resources, Methodology, Investigation, Formal analysis, Data curation, Conceptualization. **Dingding Han:** Supervision, Resources, Project administration.

Declaration of competing interest

The authors declare that they have no known competing financial interests or personal relationships that could have appeared to influence the work reported in this paper.

Acknowledgments

We acknowledge the support of the National Natural Science Foundation of China (Grant nos. 11875133, 12147101 and 11075057) and the Science and Technology Commission of Shanghai Municipality, China (Grant No. 22JC1402500). We also thank Professor Yuguo Yu and his team members for their insightful discussions.

Appendix A. Detailed P-value tables for network metrics

See Tables A.1 and A.2.

Appendix B. Explanation of parameters in the CSS formula

See Table B.1.

Table A.1
p-values for Network Metrics: During vs After (Siena Dataset). The bold values represent the smallest p-value for each metric, while the values marked with † indicate the second smallest p-value for each metric.

Network metric	wPLI	GC	PC	MSIF
Average Weighted Degree Coefficient	0.8976	0.0312	0.0236†	**0.0015**
Average Density	0.8976	0.0482	0.0236†	**0.0014**
Average Clustering Coefficient	0.3926	0.0408†	0.3282	**0.0103**
Average Diameter	0.1595†	0.2710	0.8431	**0.0507**
Average Shortest Path Length	0.2010	0.0491†	0.8726	**0.0137**
Average Degree Centrality	0.2581	0.0523†	0.7251	**0.0236**
Average Betweenness Centrality	0.3657	0.0658†	0.8936	**0.0207**
Average Closeness Centrality	0.4876	0.0816†	0.8216	**0.0403**
Average Global Efficiency	0.3984	0.1075†	0.6284	**0.0287**
Average Small World Sigma	0.4837	0.1352†	0.7523	**0.0515**
Average Modularity Coefficient	0.4927	0.2045†	0.6123	**0.0714**

Table A.2
p-values for Network Metrics: Before vs After (Siena Dataset). The bold values represent the biggest p-value for each metric, while the values marked with † indicate the second biggest p-value for each metric.

Network metric	wPLI	GC	PC	MSIF
Average Weighted Degree Coefficient	0.3356	0.3979	0.5001†	**0.5970**
Average Density	0.3356	0.4200	0.5001†	**0.7902**
Average Clustering Coefficient	0.3946	0.3536	**0.9624**	0.5588†
Average Diameter	0.2979	0.5601†	0.4348	**0.6325**
Average Shortest Path Length	0.3537	0.3827	0.5674†	**0.6989**
Average Degree Centrality	0.5489	0.5019	**0.8256**	0.7693†
Average Betweenness Centrality	0.6832	0.5502	**0.9235**	0.6890†
Average Closeness Centrality	0.7921†	0.6274	**0.9672**	0.6247
Average Global Efficiency	0.7263	0.8364†	**0.9381**	0.6912
Average Small World Sigma	0.6159	0.6910	**0.8610**	0.6912†
Average Modularity Coefficient	0.8032†	0.6731	**0.8329**	0.5421

Table B.1
Explanation of Parameters in the CSS Formula.

Parameter	Value	Description
p_1	–	p-value for the 'Before vs During' comparison.
p_2	–	p-value for the 'During vs After' comparison.
p_3	–	p-value for the 'Before vs After' comparison.
w_1	1	Weight for the 'Before vs During' comparison.
w_2	1	Weight for the 'During vs After' comparison.
w_3	1	Weight for the 'Before vs After' comparison.
γ	1	Weight for the difference term to encourage variation between p_1, p_2, and p_3.
α	0.1	Penalty coefficient for p_1 and p_2 when they exceed 0.05.
β	0.1	Penalty coefficient for p_3 when it falls below 0.05.
$I(\cdot)$	–	Indicator function that equals 1 when the condition is true, otherwise 0.

Table C.1
Optimized PSO Parameters for Weight Adjustment.

PSO Parameter	Value
Particle Count	80
Max Iterations	150
Inertia Weight	0.6 (linearly decreasing to 0.4)
Cognitive Coefficient	1.7
Social Coefficient	1.7
Velocity Limit	±0.02
Position Increment Step	0.02
Tolerance	1×10^{-6}

Table D.1
Optimized Weights for Frequency Bands, Time Windows, and Connectivity Measures for the CHB-MIT Dataset.

Weight type	Parameter	Weight value
Frequency Band Weights (α_f)	Delta (0.5–4 Hz)	$\alpha_{\text{delta}} = 0.18$
	Theta (4–8 Hz)	$\alpha_{\text{theta}} = 0.14$
	Alpha (8–13 Hz)	$\alpha_{\text{alpha}} = 0.08$
	Beta (13–30 Hz)	$\alpha_{\text{beta}} = 0.22$
	Gamma (30–100 Hz)	$\alpha_{\text{gamma}} = 0.38$
Time Window Length Weights (β_w)	1-second window	$\beta_{1s} = 0.14$
	5-second window	$\beta_{5s} = 0.56$
	10-second window	$\beta_{10s} = 0.30$
Connectivity Measure Weights (γ_m)	Weighted Phase Lag Index (wPLI)	$\gamma_{\text{wPLI}} = 0.72$
	Granger Causality (GC)	$\gamma_{\text{GC}} = 0.16$
	Peter–Clark (PC)	$\gamma_{\text{PC}} = 0.12$

Appendix C. Optimized PSO parameters for weight adjustment

See Table C.1.

Appendix D. Optimized weights for frequency bands, time windows, and connectivity measures for the CHB-MIT dataset

See Table D.1.

Data availability

The dataset can be found in the Data Acquisition and Preprocessing section.

References

[1] K.M. Fiest, K.M. Sauro, S. Wiebe, et al., Prevalence and incidence of epilepsy: a systematic review and meta-analysis of international studies, Neurology 88 (2017) 296–303.
[2] E. Beghi, G. Giussani, F. Abd-Allah, et al., Global, regional, and national burden of epilepsy, 1990–2016: a systematic analysis for the Global Burden of Disease Study 2016, Lancet Neurol. 18 (2019) 357–375.
[3] J. Engel, Seizures and Epilepsy, second ed., Contemporary Neurology Series, New York, Oxford Academic, 2013, Online edn, 1 Aug. 2013.
[4] B.C. Bernhardt, S. Hong, A. Bernasconi, N. Bernasconi, Imaging structural and functional brain networks in temporal lobe epilepsy, Front. Hum. Neurosci. 7 (2013) 624.
[5] H. Yu, J. Liu, L. Cai, J. Wang, Y. Cao, C. Hao, Functional brain networks in healthy subjects under acupuncture stimulation: An EEG study based on nonlinear synchronization likelihood analysis, Phys. A 468 (2017) 566–577.
[6] F. Lopes da Silva, EEG and MEG: relevance to neuroscience, Neuron 80 (2013) 1112–1128.
[7] D.L. Schomer, F.H. Lopes da Silva, Niedermeyer's Electroencephalography: Basic Principles, Clinical Applications, and Related Fields, Seventh ed., New York, Oxford Academic, 2017, Online edn, 1 Nov. 2017.
[8] L. Jiang, J. He, H. Pan, D. Wu, T. Jiang, J. Liu, Seizure detection algorithm based on improved functional brain network structure feature extraction, Biomed. Signal Process. Control. 79 (2023) 104053.
[9] Z. Li, K. Hwang, K. Li, et al., Graph-generative neural network for EEG-based epileptic seizure detection via discovery of dynamic brain functional connectivity, Sci. Rep. 12 (2022) 18998.
[10] E. Bullmore, O. Sporns, Complex brain networks: graph theoretical analysis of structural and functional systems, Nature Rev. Neurosci. 10 (2009) 186–198.
[11] D.S. Bassett, O. Sporns, Network neuroscience, Nature Neurosci. 20 (2017) 353–364.
[12] S. Bowyer, Coherence: a measure of the brain networks: past and present, Neuropsychiatr. Electrophysiol. 2 (2016) 1.
[13] S. Aydore, D. Pantazis, R.M. Leahy, A note on the phase locking value and its properties, NeuroImage 74 (2013) 231–244.
[14] L. Mao, G. Zheng, Y. Cai, W. Luo, Q. Zhang, W. Peng, J. Ding, X. Wang, Frontotemporal phase lag index correlates with seizure severity in patients with temporal lobe epilepsy, Front. Neurol. 13 (2022) 855842.
[15] A.K. Seth, A.B. Barrett, L. Barnett, Granger causality analysis in neuroscience and neuroimaging, J. Neurosci. 35 (2015) 3293–3297.

[16] K.J. Friston, L. Harrison, W. Penny, Dynamic causal modelling, NeuroImage 19 (2003) 1273–1302.
[17] S.I. Dimitriadis, N.A. Laskaris, V. Tsirka, M. Vourkas, S. Micheloyannis, An EEG study of brain connectivity dynamics at the resting state, Nonlinear Dyn. Psychol. Life Sci. 16 (1) (2012) 5–22.
[18] G. Zheng, Y. Li, X. Qi, et al., Mental calculation drives reliable and weak distant connectivity while music listening induces dense local connectivity, Phenomics 1 (2021) 285–298.
[19] A.M. Bastos, J. Vezoli, P. Fries, Communication through coherence with inter-areal delays, Curr. Opin. Neurobiol. 31 (2015) 173–180.
[20] X. Wang, R. Shi, X. Wu, J. Zhang, Decoding human interaction type from inter-brain synchronization by using EEG brain network, IEEE J. Biomed. Heal. Informatics 28 (1) (2024) 204–215.
[21] M. Fuscà, F. Siebenhühner, S. Wang, et al., Brain criticality predicts individual levels of inter-areal synchronization in human electrophysiological data, Nat. Commun. 14 (2023) 4736.
[22] F. De Vico Fallani, J. Richiardi, M. Chavez, S. Achard, Graph analysis of functional brain networks: practical issues in translational neuroscience, Phil. Trans. R. Soc. B 369 (2014) 20130521.
[23] T. Adamovich, I. Zakharov, A. Tabueva, et al., The thresholding problem and variability in the EEG graph network parameters, Sci. Rep. 12 (2022) 18659.
[24] H. Yu, X. Lei, Z. Song, C. Liu, J. Wang, Supervised network-based fuzzy learning of EEG signals for Alzheimer's disease identification, IEEE Trans. Fuzzy Syst. 28 (1) (2020) 60–71.
[25] H. Yu, X. Wu, L. Cai, B. Deng, J. Wang, Modulation of spectral power and functional connectivity in human brain by acupuncture stimulation, IEEE Trans. Neural Syst. Rehabil. Eng. 26 (2018) 977–986.
[26] H. Yu, X. Li, X. Lei, J. Wang, Modulation effect of acupuncture on functional brain networks and classification of its manipulation with EEG signals, IEEE Trans. Neural Syst. Rehabil. Eng. 27 (10) (2019) 1973–1984.
[27] S. Aggarwal, N. Chugh, Review of machine learning techniques for EEG based brain computer interface, Arch. Comput. Methods Eng. 29 (5) (2022) 3001–3020.
[28] E. Houssein, A. Hammad, A. Ali, Human emotion recognition from EEG-based brain–computer interface using machine learning: a comprehensive review, Neural Comput. Appl. 34 (15) (2022) 12527–12557.
[29] S. Saeedinia, M. Jahed-Motlagh, A. Tafakhori, et al., Diagnostic biomarker discovery from brain EEG data using LSTM, reservoir-SNN, and NeuCube methods in a pilot study comparing epilepsy and migraine, Sci. Rep. 14 (2024) 10667.
[30] P. Zhang, T. Li, G. Wang, C. Luo, H. Chen, J. Zhang, D. Wang, Z. Yu, Multi-source information fusion based on rough set theory: A review, Inf. Fusion 68 (2021) 85–117.
[31] Y. Liu, S. Liu, Z. Wang, A general framework for image fusion based on multi-scale transform and sparse representation, Inf. Fusion 24 (2015) 147–164.
[32] A.J. Bidgoly, et al., A survey on methods and challenges in EEG-based authentication, Comput. Secur. 93 (2020) 101788.
[33] Z. Wang, P. Mengoni, Seizure classification with selected frequency bands and EEG montages: a natural language processing approach, Brain Inform. 9 (2022) 11.
[34] A. Alzahy, M. Elgammal, H. Mohammed, H. Mostafa, Optimal EEG window size for neural seizure detection, in: 2019 8th International Conference on Modern Circuits and Systems Technologies, MOCAST, Thessaloniki, Greece, 2019, pp. 1–4.
[35] P. van Mierlo, M. Papadopoulou, E. Carrette, et al., Functional brain connectivity from EEG in epilepsy: seizure prediction and epileptogenic focus localization, Prog. Neurobiol. 121 (2014) 19–35.
[36] M. Fraschini, A. Hillebrand, M. Demuru, L. Didaci, G.L. Marcialis, An EEG-based biometric system using eigenvector centrality in resting state brain networks, IEEE Signal Process. Lett. 22 (2015) 666–670.
[37] C.A. Frantzidis, A.B. Vivas, A. Tsolaki, et al., Functional disorganization of small-world brain networks in mild Alzheimer's disease and amnestic mild cognitive impairment: an EEG study using relative wavelet entropy (RWE), Front. Aging Neurosci. 6 (2014) 224.
[38] Z. Luo, X. Lu, X. Xi, EEG feature extraction based on a bilevel network: minimum spanning tree and regional network, Electronics 9 (2020) 203.
[39] C.J. Stam, P. Tewarie, E. Van Dellen, et al., The trees and the forest: characterization of complex brain networks with minimum spanning trees, Int. J. Psychophysiol. 92 (2014) 129–138.
[40] X. Li, et al., A resting-state brain functional network study in MDD based on minimum spanning tree analysis and hierarchical clustering, Complexity 2017 (2017) 9514369.
[41] J. Gomez-Pilar, R. de Luis-García, A. Lubeiro, et al., Relations between structural and EEG-based graph metrics in healthy controls and schizophrenia patients, Hum. Brain Mapp. 39 (2018) 3152–3165.
[42] M. Lai, M. Demuru, A. Hillebrand, et al., A comparison between scalp- and source-reconstructed EEG networks, Sci. Rep. 8 (2018) 12269.
[43] Y. Zhang, et al., Predicting the symptom severity in autism spectrum disorder based on EEG metrics, IEEE Trans. Neural Syst. Rehabil. Eng. 30 (2022) 1898–1907.
[44] X. Xiong, Z. Yu, T. Ma, et al., Weighted brain network metrics for decoding action intention understanding based on EEG, Front. Hum. Neurosci. 14 (2020) 232.
[45] A. Alzahy, M. Elgammal, H. Mohammed, H. Mostafa, Optimal EEG window size for neural seizure detection, in: 2019 8th International Conference on Modern Circuits and Systems Technologies, MOCAST, IEEE, 2019, pp. 1–4.
[46] C. Gil Ávila, F.S. Bott, L. Tiemann, et al., DISCOVER-EEG: an open, fully automated EEG pipeline for biomarker discovery in clinical neuroscience, Sci. Data 10 (2023) 613.
[47] Z. Wang, P. Mengoni, Seizure classification with selected frequency bands and EEG montages: a natural language processing approach, Brain Inform. 9 (2022) 11.
[48] M.Z. Parvez, M. Paul, EEG signal classification using frequency band analysis towards epileptic seizure prediction, in: 16th Int'l Conf. Computer and Information Technology, 2014, pp. 126–130.
[49] A. Shoeb, J. Guttag, Application of machine learning to epileptic seizure detection, in: Proceedings of the 27th International Conference on Machine Learning, ICML'10, Omni Press, Madison, WI, USA, 2010, pp. 975–982.
[50] P. Detti, G. Vatti, G. Zabalo Manrique de Lara, EEG synchronization analysis for seizure prediction: A study on data of noninvasive recordings, Processes 8 (7) (2020) 846.
[51] R.W. Logan, C.A. McClung, Rhythms of life: circadian disruption and brain disorders across the lifespan, Nature Rev. Neurosci. 20 (2019) 49–65.
[52] B. Chen, C. Xu, Y. Wang, et al., A disinhibitory nigra-parafascicular pathway amplifies seizure in temporal lobe epilepsy, Nat. Commun. 11 (2020) 923.
[53] H. Yu, F. Li, J. Liu, D. Liu, H. Guo, J. Wang, G. Li, Evaluation of acupuncture efficacy in modulating brain activity with periodic-aperiodic EEG measurements, IEEE Trans. Neural Syst. Rehabil. Eng. 32 (2024) 2450–2459.
[54] H. Yu, F. Li, J. Liu, C. Liu, G. Li, J. Wang, Spatiotemporal dynamics of periodic and aperiodic brain activity under peripheral nerve stimulation with acupuncture, IEEE Trans. Neural Syst. Rehabil. Eng. 32 (2024) 3993–4003.